

## Optical-Bloch-equation method for cold-atom collisions: Cs loss from optical traps

Y. B. Band

*Department of Chemistry, Ben-Gurion University, Beer Sheva 84105, Israel  
and Institute for Theoretical Atomic and Molecular Physics, Harvard-Smithsonian Center for Astrophysics,  
60 Garden Street, Cambridge, Massachusetts 02138*

P. S. Julienne

*Molecular Spectroscopy Division, National Institute of Standards and Technology, Gaithersburg, Maryland 20899  
(Received 6 February 1992)*

We develop an optical-Bloch-equation approach for modeling ultracold-atom collisions in optical traps. The method incorporates a molecular picture of the atomic collision, laser-field dressing of the molecular states participating in the dynamics, and decay of the population and polarization due to spontaneous emission of excited states. The last is important to incorporate because the duration of the cold collisions is longer than the excited-state lifetimes. The relative motion of the atoms during the course of the collision is treated semiclassically with corrections for the time-dependent relative motion of the atoms in the various channels. An application of the method to Cs trap loss due to fine-structure-changing collisions is presented. Good agreement with experiment is obtained.

PACS number(s): 34.50.Rk, 34.50.Fa, 32.80.Pj

### I. INTRODUCTION

Rapid advances in the laser cooling and trapping of neutral atoms has led to much interest recently in collisions of ultracold trapped atoms with  $T < 1$  mK [1–14]. Collisions at such energies in the presence of nearly resonant radiation offer up a wealth of phenomena, including collective effects in collisions, extreme sensitivity to the long range of the potential, and collisions with initial conditions corresponding to mixed states with both ground- and excited-state character. Moreover, such collisions are fundamentally different from those at normal  $T$  because of the dissipative effect of excited-state spontaneous emission during the long time scale of the collision. Therefore theoretical methods are required to model and interpret these new types of experiments. Ultracold collisions can cause loss of optically confined atoms from atom traps. A good example is trap loss via fine-structure- (FS) changing collisions of alkali-metal atoms [4,8]

$$M(^2P_{3/2}) + M \rightarrow M(^2P_{1/2}) + M. \quad (1.1)$$

The fine-structure energy released is sufficient for the heated atoms to escape the atom trap. Another mechanism involves radiative escape (RE) [4,8,10],

$$M(^2P_{3/2}) + M \rightarrow M + M + \hbar\omega, \quad (1.2)$$

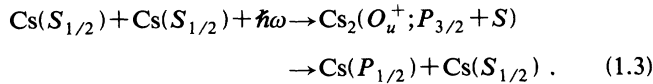
wherein a red-shifted photon is emitted in the wings of the atomic transition and the separating atoms have enough energy to escape the weak trapping forces. Trap loss based on these mechanisms has been measured [9] and calculated [8,10] for Cs atom traps, and predicted [10] for all alkali-metal species. The simple theoretical treatment of this process proposed by Gallagher and Pritchard [8] (GP) was based on weak-field perturbation

theory for exciting quasistatic distribution of ground-state atoms. Julienne and Vigué [10] (JV) generalized the GP model to treat the roles of angular momentum  $l$  and the actual molecular states instead of an effective state with averaged properties. Their picture addressed the basic question of the energy variation of the reaction rates for (1.1) and (1.2) from the normal to the ultracold regime. In this picture, dissipation has two functions: to establish the local steady-state excited population at each  $R$ , and to cause the decay of this population as it evolves to shorter distance under the accelerating influence of the upper-state potential.

We present here a simple optical-Bloch-equation (OBE) method of cold collisions in laser traps using a semiclassical treatment of the relative motion. An application of the method to Cs trap loss due to fine-structure-changing collisions is then presented. The method incorporates a molecular picture of the atomic collision, laser-field dressing of the molecular states participating in the dynamics, and population and polarization decay due to spontaneous emission. The relative motion of the atoms in the collision is treated semiclassically with corrections for the time-dependent relative motion of the atoms in the various channels. Time-dependent trajectory methods have been employed extensively in the nuclear physics literature to calculate the dynamics of the probability amplitudes for internal states of the nuclei [15]. They have also been used in atomic and molecular physics applications to model electron-atom excitation, electron-molecule excitation, and atom-molecule excitation, within the context of the time-dependent quasiclassical close-coupling approximation [16]. The correction factors incorporated here account for the widely different trajectories in the ground and excited states. Thus the cross sections and rate coefficients can be calculated so that they are *independent* of whether the ground- or

excited-state trajectories are used when suitably defined correction factors are incorporated. The OBE method has the following advantages over previous methods: (a) saturation of the trap loss rate coefficient is automatically included when the laser field is not weak, (b) multichannel aspects to the trap loss process, e.g., when both FS and RE mechanisms are simultaneously affecting the loss rate due to interactions among multiple molecular potential surfaces, can be easily treated, and (c) the OBE method does not make the steady-state approximation for the rate of optical excitation used in the JV and GP models. The consequences of the steady-state approximation as made within the JV model are investigated and found to be quantitatively inaccurate. Furthermore, the JV theory will be derived by making the steady-state approximation to the weak-field limit of the OBE for two channels.

The primary mechanism of excited-state trap loss collisions in alkali-metal atoms is fine-structure-changing collisions, which for Cs in the weak laser-field limit is



Although RE also contributes to trap loss, we consider the FS process as the example for illustrating the OBE method since it is the dominant mechanism for Cs trap loss. Radiative escape can be treated by the same method. Moreover, both processes can be calculated simultaneously using the OBE method, with the mutual effect of one on the other properly included [17]. Equation (1.3) can be viewed at weak laser fields as a three-step molecular process. In the first step, the collision on the ground  $^1\Sigma_g^+$  state of the  $\text{Cs}_2$  molecule leads to photoexcitation of the excited  $0_u^+$  state which asymptotically correlates to the  $S_{1/2} + P_{3/2}$  atomic term limit while the two Cs atoms are very far apart ( $R > 1000a_0$ ). In the second step, the excited-state population evolves from the long-range point of excitation on the  $0_u^+$  state component of the  $A^1\Sigma_u^+$  potential to  $R = R_x$ , which defines the region where a curve crossing of the  $A^1\Sigma_u^+$  and the  $b^3\Pi_u$  states occurs [ $R_x \approx 10a_0$ ]. This leads to the third step, a transition to another  $0_u^+$  state which asymptotically connects with the lower  $P_{1/2}$  fine-structure state. These processes are illustrated in Fig. 1 which shows the potential-energy surfaces involved (the  $^3\Sigma_u^+$  state which correlates to  $S_{1/2} + S_{1/2}$  does not play a role in the Cs FS-changing collisions). The ground molecular state is designated by  $g$  and the optically excited  $0_u^+$  state by  $a$ . In an ultracold collision the motion is so slow on the time scale of the excited-state lifetime,  $\tau_{ag} = 1/\gamma_{ag}$ , and the thermal energy  $kT$  is so small that both steps 1 and 2 must take into account the spontaneous emission that is responsible for natural lifetime broadening of the excited state. At strong-field strengths, both  $S_{1/2}$  and  $P_{3/2}$  atomic states are asymptotically ( $R = \infty$ ) populated, and the asymptotic state of the system must be described in terms of a mixed quantum state and is specified by a density matrix. This complicates the depiction of the first step, but the OBE treatment is fully capable of describing it.

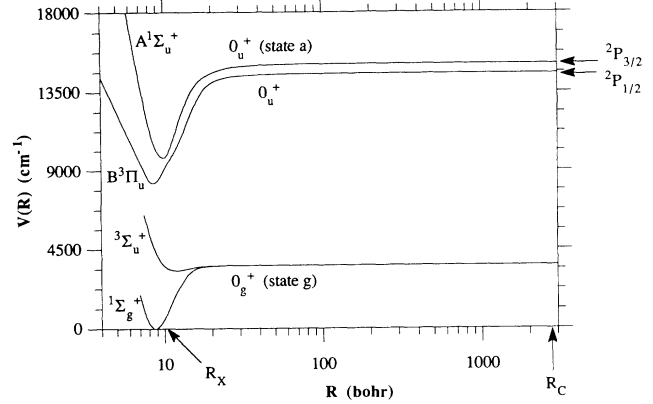


FIG. 1. Potential-energy surfaces involved in the FS-changing collisions of Cs. The ground state is designated by  $g$  and the excited state by  $a$  in the two-state description used in Sec. III.

For simplicity, we neglect the role of atomic hyperfine structure, although it will be necessary to include such structure in any complete theory. In principle, this can be done within the OBE formalism, although it greatly increases the number of channels.

Optical-Bloch-equation methods have been widely used to interpret the complex optical pumping phenomena that occur in laser cooling [18–20]. OBE's have also been applied to show how very long-range collisions (at distances comparable to the wavelength of light or more) can interrupt the process of laser cooling and put a density-dependent lower bound on the temperature which can be achieved in some cases [14].

## II. OPTICAL-BLOCH-EQUATION METHOD

In this section we explain the reasons for using a density matrix description to formulate the cold collision theory, develop the OBE technique as applied to collision phenomena, compare the OBE theory to the JV theory, and use it to derive and generalize the JV theory under the appropriate limits.

### A. Rationale for optical-Bloch-equation method

A density-matrix description of dynamics is necessary when incomplete information regarding a subsystem (comprising the colliding atoms and the laser field) results due to averaging over degrees of freedom associated with the “bath” (corresponding to the spontaneous emission degrees of freedom of the electromagnetic field). Averaging results in a mixed state of the subsystem, which cannot be described in terms of a pure state. The quantum-mechanical description of such mixed states is in terms of a density matrix [21]. The equation of motion for the density matrix is called the Liouville–von Neumann equation, or the Bloch density-matrix equation. In the context of the interaction of light with matter, OBE's have become a standard method to determine the dynamics of a system which undergoes interactions with a radiation field some of whose degrees of freedom are responsible for spontaneous emission and are reduced out of the problem [22]. The elimination of the bath degrees of

freedom leads to expressions for the lifetime of the excited states and the line shape of the transitions between the states of the subsystem [23].

The Bloch equation,  $d\rho/dt = -iL\rho$ , with the Liouville operator incorporating spontaneous emission and decay of excited-state levels, is given by

$$\frac{d}{dt}\rho = -\frac{i}{\hbar}[H(t),\rho] - \Gamma(t)\rho. \quad (2.1)$$

The decay matrix  $\Gamma(t)$  accounts for the decay of the excited-state populations and the polarizations (i.e., the off-diagonal elements of the density matrix). Written explicitly in term of components, this equation takes the form

$$\frac{d}{dt}\rho_{ij} = -\frac{i}{\hbar}[H(t)_{ik}\rho_{kj} - \rho_{ik}H(t)_{kj}] - \Gamma_{ijkl}(t)\rho_{kl}, \quad (2.2)$$

where summation convention over repeated indices is assumed, and  $i, j, k, l = 1, 2, \dots, M$ , with  $M$  equal to the number of channels used in the calculation.

### B. Practical implementation to ultracold collisions in optical traps

In our application of the OBE method to cold-atom collisions, both the Hamiltonian and the decay matrix are in general functions of time through the relative coordinate between the colliding atoms,  $R(t)$ . We define a basis set of states  $|T, l, \beta\rangle$ , where  $T$  is the entrance channel kinetic energy  $T = \hbar^2 k^2 / 2\mu$ ,  $\mu$  is the reduced mass,  $l$  is the relative angular momentum of the colliding atoms, and  $\beta$  is an adiabatic channel index. The adiabatic channel is taken to be a state of the molecule and the laser field. The matter-field coupling operator  $H_{\text{int}}(t) = -E(x, t)\mu$  is not included in obtaining the adiabatic channel basis. Here,  $E(x, t)$  is taken to be a single-mode electric field which is nearly in resonance with an asymptotic atomic transition, and is given by

$$E(x, t) = \{ A \exp[i(kx - \omega t)] + \text{c.c.} \} / 2, \quad (2.3)$$

and  $\mu$  is the transition dipole moment matrix for the system in the adiabatic channel basis. In the electric dipole approximation  $\exp[i(kx)]$  is taken to be unity [24], but retardation effects can become important and lead to the breakdown of the dipole approximation [10] (this can be easily included within the present formalism). The matter-field coupling operator is often expressed in terms of the Rabi frequencies for the adiabatic channels,  $\Omega_{ij}(t) = A\mu_{ij}(R(t))/\hbar$ , where  $\mu_{ij}$  is the transition dipole moment between adiabatic states  $i$  and  $j$ . The Hamiltonian matrix elements take the form

$$\begin{aligned} H_{ij}(t) &= H_{0,ij}(t) - E(t)\mu_{ij} \\ &= H_{0,ij}(R(t)) - \hbar\Omega_{ij}(t)e^{-i\omega t} - \hbar\Omega_{ij}^*(t)e^{i\omega t}. \end{aligned}$$

Upon expanding the elements of the density matrix,  $\rho_{ij}$ , in slowly varying envelopes which oscillate at Fourier frequencies  $m\omega$ ,  $\rho_{ij}^{(m)}$ , and making the rotating-wave approximation, we obtain the set of equations governing the dynamics of the system [25,26].

As an example, let us take a two-channel case with a ground-state molecular state ( $g$ ) and an excited molecular state ( $a$ ), coupled to the ground-state channel via the laser field. The two adiabatic channels,  $|1\rangle$  and  $|2\rangle$ , are given by  $|1\rangle = |g, N\rangle$  and  $|2\rangle = |a, N-1\rangle$ , where the second index indicates the number of photons in the laser field. The zero-order molecule plus laser-field Hamiltonian is given by

$$\mathbf{H}_0(t) = \begin{bmatrix} \varepsilon_g(R(t)) + N\hbar\omega & 0 \\ 0 & \varepsilon_a(R(t)) + (N-1)\hbar\omega \end{bmatrix}, \quad (2.4)$$

where

$$\varepsilon_i(R(t)) = V_i(R(t)) + \hbar^2 l(l+1)/2\mu R(t)^2. \quad (2.5)$$

The matter-field interaction Hamiltonian is given by

$$\mathbf{H}_{\text{int}}(t) = -\hbar \begin{bmatrix} 0 & \tilde{\Omega}(R(t)) \\ \tilde{\Omega}(R(t)) & 0 \end{bmatrix}, \quad (2.6)$$

where

$$\tilde{\Omega}(R(t)) = \langle 1 | E(t)\mu(R(t)) | 2 \rangle / \hbar. \quad (2.7)$$

$\mathbf{H}_{\text{int}}(t)$  has components which oscillate with  $e^{-i\omega t}$  and  $e^{i\omega t}$ , whereas  $\mathbf{H}_0(t)$  oscillates with  $e^{im\omega t}$  with  $m=0$ , i.e., it does not oscillate. The density-matrix equations are given by [25,26]

$$\begin{aligned} i\partial_t \rho_{21}^{(1)} &= [\omega_{21}(R(t)) - \omega - i\Gamma_{ag}(R(t))] \rho_{21}^{(1)} \\ &\quad - \Omega(R(t))(\rho_{11}^{(0)} - \rho_{22}^{(0)}), \\ i\partial_t \rho_{22}^{(0)} &= [\Omega(R(t))^* \rho_{21}^{(1)} - \text{c.c.}] - i\gamma_{ga} \rho_{22}^{(0)}, \\ i\partial_t \rho_{11}^{(0)} &= -[\Omega(R(t))^* \rho_{21}^{(1)} - \text{c.c.}] + i\gamma_{ga} \rho_{22}^{(0)}, \end{aligned} \quad (2.8)$$

where  $\Gamma_{ag}$  is the decay rate of the polarization  $\rho_{21}^{(1)}$ , and  $\gamma_{ga}$  is the decay rate of the population  $\rho_{22}^{(0)}$ , and  $\omega_{21}(R(t)) = [\varepsilon_a(R(t)) - \varepsilon_g(R(t))]/\hbar$  is the difference of the two molecular potentials. We take  $\Gamma_{ag} = \gamma_{ga}/2$ , i.e., no proper  $T_2$  decay is necessary [21]. For the present application to Cs, the decay rates are taken to be independent of internuclear coordinate and given by  $\gamma_{ga} = \frac{4}{3}\gamma_A$  for the  $0_u^+$  state [10], where  $\gamma_A = (30 \times 10^{-9} \text{ s})^{-1}$  is the atomic decay rate. For notational simplicity we shall refer to  $\rho_{11}^{(0)}$ ,  $\rho_{22}^{(0)}$ , and  $\rho_{21}^{(1)}$  as  $\rho_{gg}$ ,  $\rho_{aa}$ , and  $\rho_{ag}$ , respectively.

Steady-state expressions for the density matrix can be easily obtained at any given value of  $R$  by setting the time derivatives in Eqs. (2.2) equal to zero. One thereby obtains, after some algebra,

$$\begin{aligned} \rho_{aa}^{\text{SS}} &= \frac{|\Omega(R)|^2}{\{[\omega_{21}(R) - \omega]^2 + \Gamma_{ag}(R)^2\} \gamma_{ga}(R) / 2\Gamma_{ag}(R) + 2|\Omega(R)|^2}, \\ \rho_{ag}^{\text{SS}} &= \frac{\Omega(R)}{[\omega_{21}(R) - \omega - i\Gamma_{ag}(R)]} (1 - 2\rho_{aa}^{\text{SS}}). \end{aligned} \quad (2.9)$$

In the limit of small Rabi frequency these expressions reduce to

$$\begin{aligned}\rho_{aa}^{SS} &= \frac{|\Omega(R)|^2}{[\omega_{21}(R) - \omega]^2 + \gamma_{ga}(R)^2/4}, \\ \rho_{ag}^{SS} &= \frac{\Omega(R)}{\omega_{21}(R) - \omega - i\gamma_{ga}(R)/2},\end{aligned}\quad (2.10)$$

where we have taken  $\gamma_{ga}(R)/\Gamma_{ag}(R) = 2$ . This reduces to the standard two-level result asymptotically where the Rabi frequency and the decay parameters reduce to their  $R \rightarrow \infty$  values.

For the case with a ground-state molecular channel  $g$  and two excited electronic state molecular channels coupled to the ground-state channel via the laser field, which we call  $a$  and  $a'$ , the three adiabatic channels  $|1\rangle$ ,  $|2\rangle$ , and  $|3\rangle$  are given by  $|1\rangle = |g, N\rangle$ ,  $|2\rangle = |a, N-1\rangle$ , and  $|3\rangle = |a', N-1\rangle$ . The zero-order molecule plus laser-field Hamiltonian is given by

$$H_0(t) = \begin{pmatrix} \varepsilon_1(R(t)) + N\hbar\omega & 0 & 0 \\ 0 & \varepsilon(R(t)) + (N-1)\hbar\omega & 0 \\ 0 & 0 & \varepsilon_3(R(t)) + (N-1)\hbar\omega \end{pmatrix}, \quad (2.11)$$

and the matter-field interaction Hamiltonian is

$$H_{\text{int}}(t) = -\hbar \begin{pmatrix} 0 & \Omega_{12}(R(t)) & \Omega_{12}(R(t)) \\ \Omega_{12}(R(t)) & 0 & 0 \\ \Omega_{13}(R(t)) & 0 & 0 \end{pmatrix}. \quad (2.12)$$

The density-matrix equations for  $\rho_{11}^{(0)}$ ,  $\rho_{22}^{(0)}$ ,  $\rho_{33}^{(0)}$ ,  $\rho_{12}^{(1)}$ ,  $\rho_{13}^{(1)}$ , and  $\rho_{23}^{(0)}$ , similar to Eqs. (8)–(10), are easily obtained. Generalization to more than three channels, and arbitrary radiative couplings between the channels is also readily accomplished.

In order to solve the density-matrix equations,

$$\frac{d}{dt}\rho_{ij} = -iL_{ijkl}(t)\rho_{kl}, \quad (2.2')$$

the classical trajectory  $R(t)$  must be known, since the dipole moment, the molecular energies, and in general, the decay rates are functions of time through the relative coordinate. If we take the relative coordinate to be propagated on a reference potential surface,  $\varepsilon_0(R)$ ,

$$\frac{dR}{dt} = \{2\mu[T - \varepsilon_0(R(t))]\}^{1/2}, \quad (2.13)$$

where  $T$  denotes the asymptotic relative kinetic energy of the cold atoms, and if we take this same trajectory for all channels to be this reference trajectory, the flux on a given channel  $k$  will not have the correct motion. In order to correct for this, we replace Eq. (2.2') by

$$\frac{d}{dt}\rho_{ij} = -iL_{ijkl}(t)\rho_{kl}C_k(t)C_l(t), \quad (2.2'')$$

where the correction factors  $C_k(t)$  are given by

$$C_k(t) = \left\{ \frac{\{T - [\varepsilon_0(R(t)) - \varepsilon_0(\infty)]\}}{\{T - [\varepsilon_k(R(t)) - \varepsilon_k(\infty)]\}} \right\}^{1/4}. \quad (2.14)$$

These factors correct the terms in the equations for the different velocities on the different channels. We shall explicitly demonstrate for the cases under study that the arbitrary choice of propagating the trajectory  $R(t)$  on any particular channel, say channel 1, and using the correction factors with channel 1 used as the reference channel, produces results identical with those obtained by choosing any other channel upon which to propagate  $R(t)$ , say channel  $\alpha$ , and using the correction factors with channel  $\alpha$  used as the reference channel. Hence it really does not matter what trajectory is chosen. The choice is entirely arbitrary and the results are insensitive to the choice. Otherwise, no justification for choosing a particular trajectory could be made. The correction factors  $C_k$  are designed to go to unity at large internuclear separation, so that when  $R$  is large Eq. (2.2'') reduces to (2.2'). These correction factors have been used in the quasiclassical close-coupling approximation for probability amplitudes [16] to obtain trajectory-independent results.

A heuristic explanation of these correction factors is as follows. At a given value of  $R$ , the local velocities on different channels are of course different. But this is not accounted for in Eq. (2.2') for the rate of change of the density matrix. Hence we multiply the terms on the right-hand side of Eq. (2.2') proportional to  $\rho_{kk}$  by  $C_k(t)C_k(t)$  to account for the fact that the velocity in channel  $k$  is different from the velocity of the reference channel. Thus, if at a given  $R$ , channel  $k$  has a turning point nearby, the contribution to the rates from the terms with  $\rho_{kk}$  will be enhanced because  $C_k(t)C_k(t)$  becomes large. The form of the correction factor is motivated by the WKB amplitude of the wave function which relates to how much classical time is spent near a given value of  $R$ . The correction factors modify the dynamics of the density matrix so as to correspond to calculating a trajectory-independent value of the density matrix  $\rho_{ij}(R)$ . This can easily be seen by computing  $d\rho_{ij}/dR$ , which, from the expression

$$\begin{aligned}
\frac{d\rho_{ij}}{dR} &= \frac{d\rho_{ij}}{dt_0} \left[ \frac{dt_0}{dR} \right] = -iL_{ijkl}(t)\rho_{kl}C_k(t)C_l(t) \frac{1}{v_0(t)} \\
&= -iL_{ijkl}\rho_{kl} [2\mu\{T - [\varepsilon_k(R(t)) - \varepsilon_k(\infty)]\} 2\mu\{T - [\varepsilon_l(R(t)) - \varepsilon_l(\infty)]\}]^{-1/4} \\
&= -iL_{ijkl}\rho_{kl} [v_k(R)v_l(R)]^{-1/2}, \tag{2.15}
\end{aligned}$$

is clearly independent of any reference trajectory; hence  $\rho_{ij}(R)$  is trajectory independent. Thus one need only compute Eq. (2.15) and trajectory equations need not be used, i.e., one need not compute (2.2'') together with (2.13), and therefore  $\rho_{ij}(R)$  is trajectory independent. Note also that without decay terms present, the density matrix computed using Eq. (2.15) remains idempotent. Furthermore, with the decay terms such that state  $a$  decays only to state  $g$ , and no decay out of the two-level manifold is present, the density matrix computed using Eq. (2.15) also remains idempotent. A comparison of results using (2.15), close-coupled calculations, and wavepacket density matrix calculations with the kinetic-energy part of the Hamiltonian treated as an operator will be presented elsewhere. We should mention that the terms  $v_k(R)^{-1/2} = [2\mu\{T - [\varepsilon_k(R) - \varepsilon_k(\infty)]\}]^{-1/4}$ , which become singular near a turning point because the local channel velocity goes to zero, can be regularized by replacing them with amplitudes  $A_k(R)$  obtained from uniform WKB wave functions [27].

Before beginning the propagation of Eqs. (2.2'') and (2.13) [or Eq. (2.15)], we must obtain the asymptotic density matrix  $\rho(t=0)$  [or  $\rho(R=\text{large})$ ], which serves as an initial condition for the OBE, Eqs. (2.2''). To do so, we perform an initial calculation by setting  $R(t=0)$  equal to a large value (where the channel potential is very close to its asymptotic value), and propagating the density-matrix equation (2.13) with initial condition  $\rho_{ij}(t=0) = \delta_{i1}\delta_{j1}$  (i.e., the system is in the lowest molecular state asymptotically), together with the coordinate with zero velocity,  $dR/dt=0$ , until a steady-state value of the density matrix is obtained. This procedure guarantees that the steady-state asymptotic density matrix is obtained at large  $R$ . The resulting density matrix is used as the initial condition for the OBE equation (2.15) [or Eq. (2.2'')] which is solved together with the trajectory equation (2.13) with nonvanishing right-hand side, and the actual propagation as a function of relative coordinate begins.

### C. OBE theory of cold FS-changing collisions

The event rate  $R(T)$  for the FS transition in the OBE theory is given by

$$\begin{aligned}
R(T) &= K_g N^2 = \frac{1}{2g^2} \frac{\pi v}{k^2} \sum_l (2l+1) P_X(l) \\
&\quad \times \rho_{aa}(R_X, l, \Delta, \phi) N^2, \tag{2.16}
\end{aligned}$$

where  $N$  is the atomic density,  $v = \hbar k / \mu$  is the asymptotic velocity,  $g=2$  is the ground-state degeneracy (for  $^2S_{1/2}$  neglecting hyperfine structure), both even and odd partial waves contribute to the sum, and the symmetry factor of  $\frac{1}{2}$  accounts for homonuclear symmetry. All effects of ex-

citation and survival due to steps 1 and 2 in Eq. (1.3) are accounted for by the excited-state population,  $\rho_{aa}(R_X, l, \Delta, \phi)$ , which gives the total probability at  $R=R_X$  that the molecule is found in the upper state due to propagation in the region  $R > R_X$ . The molecule interacts in this region with radiation detuned by  $\Delta = \omega - \omega_0$  from the atomic resonance frequency  $\omega_0$ , with photon flux  $\phi$  ( $\phi = I/\hbar\omega$ , where  $I$  is the laser intensity). The structure of expression (2.16) looks like an ordinary rate coefficient in which the colliding ground-state atoms are converted to the  $P_{1/2} + S$  product atoms by a sequential process involving two probabilities, first  $\rho_{aa}(R_X, l, \Delta, \phi)$  for excitation and survival, then  $P_X$  for the FS transition itself. The probability  $P_X$  was calculated quantum mechanically by JV. In some cases it is well approximated by the Landau-Zener probability at an isolated crossing, though more generally,  $R_X$  merely indicates a region in which the nonadiabatic quantum-mechanical coupling occurs.

### D. Julienne-Vigue theory of cold FS-changing collisions

In the JV theory, the excitation in step 1 of the FS-changing collision represented by Eq. (1.3) occurs from a distribution of approaching atoms between  $R$  and  $R+dR$  with relative angular momentum  $l$  and collision kinetic energy  $E_k$ . The excitation rate  $G_{ga}^{JV}(R)$  is given by the weak-field photoabsorption cross section,

$$G_{ga}^{JV}(R) = \sigma_{ga}(R, \Delta) \phi = \sigma_{ga}^{\text{peak}} \chi_{ga}(R, \Delta) \phi, \tag{2.17}$$

where  $\sigma_{ga}^{\text{peak}}$  is the peak photoabsorption cross section,  $\sigma_{ga}^{\text{peak}} = \lambda^2/2\pi$ , and  $\chi_{ga}(R, \Delta)$  is the  $R$ -dependent Lorentzian line-shape function normalized to unity at the peak,  $\delta(R_C) = 0$ :

$$\chi_{ga}(R, \Delta) = \{1 + [2\delta(R)/\gamma_{ag}]^2\}^{-1}. \tag{2.18}$$

Here  $\delta(R)$  is the detuning from the molecular resonance frequency  $\omega_{21}(R)$ , given by the  $R$ -dependent difference between the upper and lower molecular potentials

$$\hbar\omega_{21}(R) = \hbar\omega + \hbar\delta(R). \tag{2.19}$$

In the conventional quasistatic picture, absorption only occurs at the Condon point  $R_C(\Delta)$  where the molecule is in resonance with the light, i.e.,  $\omega_{21}(R_C) = \omega$  or  $\delta(R_C) = 0$ . Since the excitation step occurs in the long-range part of the molecular potentials, where the ground-state potential is flat and the excited-state potential varies as  $-C_3/R^3$ , then  $R_C = (C_3/\hbar\Delta)^{1/3}$ . In the ultracold theories of GP and JV, off-resonant excitation when  $R$  is much smaller than the Condon point is also

important, since the excited atoms are less likely to decay by spontaneous emission if they are excited when they are closer together.

The second step of the process in Eq. (1.3) is strongly influenced by excited-state decay during the long propagation time from the long-range  $R$  of excitation to the crossing at  $R_X \approx 10a_0$ . The excited-state population which survives decay during this propagation is calculated semiclassically by

$$S_a(R_X, R, l) = \exp \left[ - \int_{R_X}^R \frac{\gamma_{ag}(R')}{v_a(R', l)} dR' \right], \quad (2.20)$$

where the trajectory is chosen for motion on the excited-state potential  $a$ , and hence the velocity is taken as  $v_a(R', l)$ . There are ambiguities about the choice of this trajectory that have been discussed by JV, and we will also discuss these in Sec. II E below.

The third step, the FS transition at the  $R_X$  crossing, is described by a probability  $P_X(l)$  that for the case of Cs is nearly independent of incident collision energy between room temperature and  $T \rightarrow 0$  [10]. This probability can be calculated quantum mechanically or semiclassically, and is 0.43 for the Cs FS transition [10].

The event rate  $R(T)$  for the FS transition in the JV theory is

$$R^{JV}(T) = K_g N^2 = \frac{1}{2g^2} \frac{\pi v}{k^2} \sum_l (2l+1) P_X(l) \times P_{ga}^{JV}(R_X, l, \Delta, \phi) N^2, \quad (2.21)$$

where here  $N$  is the ground-state density. The effects due to steps 1 and 2 of Eq. (1.3) are accounted for by the excitation/survival factor,  $P_{ga}(R_X, l, \Delta, \phi)$ . In Eq. (2.21), the colliding ground-state atoms are converted to the  $P_{1/2} + S$  product atoms by a sequential process involving two probabilities, first  $P_{ga}$  for excitation followed by survival, then  $P_X$  [the same  $P_X$  as in Eq. (2.16)] for the FS transition itself. The factor  $P_{ga}^{JV}(R, l, \Delta, \phi)$  gives the total probability that the upper state will be excited at some  $R'$  and survive to  $R$ :

$$P_{ga}^{JV}(R, l, \Delta, \phi) = \int_R^\infty G_{ga}^{JV}(R') S_a(R, R', l) dR' / v(R', l). \quad (2.22)$$

The smallest  $R'$  at which excitation is possible is the classical turning point on the ground-state potential for collisions with relative angular momentum  $l$ ; although  $v(R', l)$  vanishes at this  $R'$ , the singularity in Eq. (2.22) is integrable. Note that the semiclassical probability in Eq. (2.22) should be interpreted as a dynamically determined probability that is the consequence of motion on two trajectories. The term  $dR'/v(R', l)$  in Eq. (2.22) is the classical time spent in the ground state in  $dR'$ , and gives the amount of time spent absorbing at rate  $G_{ga}^{JV}(R')$ . It depends on the ground-state trajectory. On the other hand, the survival factor  $S_a$  depends solely on the trajectory on the excited-state potential. In our OBE formulation the effect of *both* trajectories is included by using the correction factors described in Sec. II B. The integral probability in Eq. (2.22) simply reflects the probability of being ex-

cited to state  $a$  at  $R'$  then surviving on  $a$  to  $R$ . Thus, we see that the JV theory is actually a dynamical theory, although it was originally derived as if it were a quasistatic theory.

If we assume that  $v$  is large compared to the characteristic velocity  $v_S$  where the atoms move a distance  $\omega/c = \lambda/2\pi$  in one natural lifetime  $\tau_{ga}$ , then excited-state decay during the collision can be ignored. In this limit the integrand comes almost entirely from long-range excitation, where  $R \gg \lambda/2\pi$ , the parameters take on their atomic values, and a simple limit is obtained [10]. The integral in Eq. (2.22) becomes

$$P_{ga}(R, l, \Delta, \phi) = G_A \int_{R_X}^R \exp[-\gamma_A R'/v] dR' / v = G_A / \gamma_A = f^*, \quad (2.23)$$

where  $G_A$  is the atomic excitation rate and  $f^*$  is the weak-field excited-state fraction. In evaluating (2.23) we used the asymptotic limit  $\gamma_{ga} = \gamma_A$  [28], and take  $R_X = 0$ , since  $R_X \ll v/\gamma_A$ , the distance moved in a lifetime. Thus the FS rate in this limit is

$$R(t) = K_g N^2 = K^* f^* N^2 = K^* N N^*, \quad (2.24)$$

where  $K^*$  is now the conventional excited-state rate coefficient. The consequence of having an ultracold collision with  $v \ll v_S$  is to move the excitation-survival process from the atomic region,  $R \gg \lambda/2\pi$ , into the long-range molecular region  $R < \lambda/2\pi$ , where molecular excitation and survival control the  $P_{ga}$  integral. Although in the usual quasistatic theory the excitation is normally thought to occur at the Condon point, the off-resonant line-shape function in Eq. (2.18) allows excitation over a wide range of  $R$ . In fact, JV showed that the rate for Cs FS collisions at ultracold  $T$  comes primarily from distance  $R$  much less than  $R_C$ , because the greatly improved survival probability compensates for the smaller off-resonance excitation rate. The effect of the off-resonance line shape cannot be taken into account by standard quantum collision theory based on calculating wave functions, which assumes a conservative Hamiltonian, not a dissipative system. However, the OBE method readily handles the effect of dissipation.

### E. Incorporation of OBE results into JV theory

We will now apply the semiclassical OBE theory to improve the JV description of the collision and obtain a better understanding of these novel collisions. We will continue to work within the framework of a two-state approximation, using the relevant molecular potentials.

The density matrix  $\rho_{aa}(R, l, \Delta, \phi)$  represents the probability of being in the excited state at  $R$ , given motion along the trajectory from  $R = \infty$  with angular momentum  $l$ , detuning  $\Delta$ , and photon flux  $\phi$ . But this same probability in the JV theory is given by  $P_{ga}(R, l, \Delta, \phi)$  from Eq. (2.22), which integrates the excitation and/or survival from  $R' = \infty$ . Therefore  $P_{ga}$  and  $\rho_{aa}$  can be compared directly. Also, the OBE version of the rate constant, Eq. (7), is found by using  $\rho_{aa}(R_X)$  instead of  $P_{ga}(R_X)$ . The JV expression for  $P_{ga}(R)$ , from Eq. (2.22),

uses the local steady-state excitation rate  $G_{ga}(R')$  found by making a steady-state approximation to the OBE's. The OBE equation for  $\partial_t \rho_{aa}$  is

$$\partial_t \rho_{aa} = 2\Omega \text{Imp} \rho_{ga} - \gamma_{ga} \rho_{aa}, \quad (2.25)$$

for which the excitation rate at  $R$  in steady state is

$$\begin{aligned} G_{ga}(R') &\equiv 2\Omega \text{Imp} \rho_{ag}^{\text{SS}}(R') \\ &= \gamma_{ga} \rho_{aa}^{\text{SS}} \\ &= \gamma_{ga} \frac{\Omega(R')^2}{\delta(R')^2 + [\gamma_{ga}(R')/2]^2 + 2\Omega(R')^2} \\ &\rightarrow \gamma_{ga} \frac{\Omega(R')^2}{\delta(R')^2 + [\gamma_{ga}(R')/2]^2} = G_{ga}^{\text{JV}}(R') \end{aligned} \quad (2.26)$$

in the weak-field limit. The weak-field excitation rate of JV, Eq. (2.17), is equivalent to Eq. (2.26) given that

$$\Omega(R')^2 = \frac{\lambda^2}{8\pi} \gamma_{ga}(R') \phi = \frac{1}{4} \sigma_{ga}^{\text{peak}} \gamma_{ga}(R') \phi. \quad (2.27)$$

Equation (2.26) immediately suggests another approximation which should be compared to the full OBE results for  $\rho_{aa}(R)$ . Instead of using the local steady-state solution  $G_{ga}(R')$  for the excitation rate in Eq. (2.22), use instead the actual *calculated* rate,

$$G_{ga}^{\text{OBE}}(R') = 2\Omega \text{Imp} \rho_{ga}(R'), \quad (2.28)$$

from the numerical OBE solutions for the given  $l$ ,  $\Delta$ , and  $\phi$  to calculate  $P_{ga}^{\text{OBE}}$ . Therefore we have three quantities which will be directly compared in the figures, the numerical  $\rho_{aa}(R)$ , the quantity  $P_{ga}^{\text{JV}}(R)$  calculated from Eq. (2.22) using  $G_{ga}^{\text{JV}}(R') = G_{ga}^{\text{SS}}(R)$ , and the quantity  $P_{ga}^{\text{OBE}}(R)$  calculated from Eq. (2.22) using  $G_{ga}^{\text{OBE}}(R)$  instead of  $G_{ga}^{\text{JV}}(R')$ . When  $R$  is so large that all quantities no longer depend on  $R$ , Eq. (2.23) can be written as

$$P_{ga}(R, l, \Delta, \phi) \approx \rho_{aa}^{\text{SS}}(\infty), \quad (2.29)$$

by using Eq. (2.26). So we see that the JV integral, Eq. (2.22), goes to the OBE steady-state solution if neither the potential nor detuning are dependent on  $R$  in the limit of small intensities where saturation effects do not play a role.

One other pleasing weak-field limit can be deduced from the form in (2.26). When the detuning  $\Delta$  is comparable to  $\gamma_{ga}$ , the region of excitation in the integrand of (2.22) is spread out over a wide range, on the order for  $v/\gamma_{ga}$ . On the other hand, when the detuning is large,  $\Delta \gg \gamma_{ga}$  [29], the excitation is concentrated in a narrow region about the Condon point  $R_C(\Delta)$ , having a width of about  $\gamma_{ga}/D_C$ , where

$$D_C = \frac{d\omega_{21}(R_C)}{dR} = \frac{d\delta(R_C)}{dR}. \quad (2.30)$$

Using the linearizing approximation  $dR = d\delta/D_C$  near  $R_C$ , integration over the rapidly varying line shape in (2.22) can immediately be done to give

$$P_{ga}^{\text{JV}}(R, l, \Delta \gg \gamma_{ga}, \phi) = 2\pi \frac{|\hbar\Omega(R_C)|^2}{\hbar^2 D_C v(R_C)} S_a(R, R', l). \quad (2.31)$$

But the expression multiplying  $S_a$  is just the *single* pass Landau-Zener curve hopping probability that a transition occurs at the Condon point from the  $g$  to the  $a$  diagonal molecule-field potentials in (2.4) under the influence of the field-induced coupling in (2.6). This shows that the spontaneous emission width drops out of the excitation probability when the excitation region is well localized, and the conventional scattering-in-fields picture of the collision applies, though now modified by the probability  $< 1$  of survival on the excited state.

There is an additional problem which needs to be addressed in relating the OBE and JV theories, namely, how to choose the excited-state trajectory used in computing the correction factors in the OBE theory. Both JV [10] and Gallagher [13] have discussed the problem of choosing excited-state trajectories in ultracold collisions. If the excitation occurs when the atoms are very far apart and noninteracting, then clearly both states  $g$  and  $a$  evolve with the same velocity and the initial kinetic energy of the excited state is the same as in the ground state:  $T_a(\infty) = T_g(\infty)$ , where we are using the notation  $T_k(R) = T - \varepsilon_k(R) = (\mu/2)[v_k(R)]^2$ . Overall energy conservation is satisfied when Rayleigh scattering occurs since the emitted photon has the same frequency as the incident photon (we omit laser cooling considerations here). On the other hand, when a molecular transition occurs during a conventional collision in a radiation field, energy conservation dictates that the excited state has asymptotic kinetic energy  $T_a(\infty) = T_g(\infty) + \hbar\Delta$ . Overall energy conservation is satisfied since the frequency of the light emitted after the collision is the atomic transition frequency  $\omega_0 = \omega - \Delta$ . This is the familiar process of the collisional redistribution of light [30,31]. When an ultracold collision occurs, the finite excited-state lifetime leads to off-resonant excitation during the collision, leading to a spread of energy in the excited-state wave packet. If the detuning is much greater than  $\gamma_{ga}$ , Eq. (2.31) above shows that the lifetime broadening effect is negligible and the transition is localized near the Condon point  $R_C(\Delta)$ . Conventional energy conservation applies, and choosing the excited-state trajectory according to  $T_a(\infty) = T_g(\infty) + \hbar\Delta$  ensures that the classical Franck-Condon principle (CFCP) is satisfied at the Condon point, that is, the excited-state velocity after the transition,  $v_a(R_C)$ , is the same as the ground-state velocity  $v_g(R_C)$  before the transition.

For small detuning  $\Delta$  on the order of  $\gamma_{ga}$  the excitation is delocalized, and the CFCP is *only* satisfied at  $R_C$  if the conventional energy conserving trajectory is chosen. Because of the pleasing physical picture behind the CFCP, i.e., no sudden velocity jumps occur in the semiclassical picture when the photon is absorbed at a particular point on the trajectory, both JV and Gallagher [13] argue that it may be a good approximation for off-resonance excitation in ultracold collisions. Enforcing the CFCP creates an excited-state wave packet with a spread of energy. JV found better agreement with the measured Cs trap loss experiment [9] when the CFCP was used for choosing the initial excited-state velocity for calculating the survival integrals.

### F. Correction-factor modifications

In our OBE theory there is no identifiable “point” at which a photon transition occurs, rather, the density matrix evolves in time under the influence of radiative and interatomic interactions. However, the trajectories, which define the time dependence and the correction factors, must be preselected according to some criterion. Our results for the density matrix are independent of whether ground- or excited-state trajectories are used, but the final density matrix does depend on the criterion used to select the excited-state trajectories. This is one of the limitations of the semiclassical OBE method. One choice we make is  $T_a(\infty) = T_g(\infty)$ , so the asymptotic velocities in the ground and excited states are the same. We call this the asymptotic trajectory choice. In this case, the correction factors all go to unity as  $R \rightarrow \infty$ . This choice does not satisfy the CFCP at  $R_C$ , and tends to make the survival factors too large, since the velocity will be too large as the atoms come together. A second choice, which we designate energy conserving, uses the energy conserving excited-state trajectory, hence  $T_a(\infty) = T_g(\infty) + \hbar\Delta$ . This satisfies the CFCP at  $R_C$  but gives unphysical correction factors  $\neq 1$  as  $R \rightarrow \infty$ . A third choice is a hybrid trajectory for calculating the excited-state correction factors, namely, one which is the ground-state trajectory for  $R > R_C$  and switches to the conventional energy conserving trajectory for  $R < R_C$ . We call this the switched trajectory choice. This satisfies the CFCP at  $R = \infty$  and at  $R = R_C$ , though not elsewhere, and has unit correction factors for  $R > R_C$ . The switched correction factor choice takes the velocity on the excited-state trajectory equal to

$$v_a(R) = \begin{cases} v_g(R) & \text{for } R > R_C \\ [2\mu\{T - [\varepsilon_a(R) - \varepsilon_a(\infty) - \hbar\Delta]\}]^{1/2} & \text{for } R \leq R_C \end{cases} \quad (2.32)$$

It leads to the right result, Eq. (2.31) for the case of large red detuning, and hopefully is reasonably correct for small detuning also. Table I summarizes the kinetic energies at  $R = \infty$  and  $R = R_C$  for the three choices.

In order to solve the problems associated with the spread of the wave packet in space and energy, it is necessary to use a fully quantal, rather than semiclassical, formalism. A time-dependent density-matrix approach is needed with the kinetic energy treated as an operator [32], i.e.,

$$\frac{d}{dt}\rho(R, R'; t) = -\frac{i}{\hbar}[H(R)\rho(R, R'; t) - \rho(R, R'; t)H(R')] - \Gamma\rho, \quad (2.33)$$

where the Hamiltonian matrix operator  $H(R)$

$= T(R)1 + V(R)$  is a differential operator because of the nuclear-kinetic energy term. Some preliminary treatment along these lines has been given for very long-range collisions by Smith and Burnett [14] and for trap loss collisions by Julienne, Smith, and Burnett [33]. The present OBE approach is only an approximation to the full density-matrix treatment of Eq. (2.33) and the relevant physics of the relative motion has to be properly built in. The full treatment will yield a continuous distribution of asymptotic kinetic energies centered around  $T_g(\infty)$  and also centered around  $T_g(\infty) + \hbar\Delta$ .

### III. CS FINE-STRUCTURE-CHANGING COLLISIONS

We will now test the OBE theory and compare it against experiment and against the JV theory. In the calculations reported here we only consider FS-changing collisions. This is the dominant mechanism for trap loss of Cs for small detunings and low laser intensities. In planned publications we will report calculations including both FS-changing collisions and RE for a number of alkali-metal atoms.

#### A. Calculated density-matrix elements

Initially, we consider calculations at low laser intensity, where saturation effects are unimportant. The laser intensity is taken to be  $1.4 \times 10^{-5}$  W/cm<sup>2</sup>. The laser frequency detuning  $\Delta/2\pi$  is taken to be equal to Cs <sup>2</sup>P excited-state decay width  $\gamma_{ga}/2\pi = 5.3$  MHz, i.e.,  $\Delta/2\pi = [\omega - \omega_0] = -5.3$  MHz. The calculation is performed for a kinetic energy corresponding to a temperature of 0.3 mK ( $T = 9.5 \times 10^{-10}$  hartree). We first consider the relative angular momentum  $l=0$  channel. In these calculations we shall first use the asymptotic correction factor choice. The same excited-state trajectory was chosen to calculate the survival factor in making comparison with the  $P_{ga}$  calculated from Eq. (2.22).

Figure 2 shows the calculated excited-state population  $\rho_{aa}(R, l, \Delta, \phi)$  versus internuclear distance  $R$  for the values of  $l$ ,  $\Delta$ , and  $\phi$  specified above. We started the propagation of the density matrix at  $R = 4000$  bohrs with the equilibrium density matrix given in Eq. (2.9). Crossing of the ground state  $g$  [<sup>1</sup> $\Sigma_g + \hbar\omega$ ] and the excited state [ $0_u^+$ ] occurs at the Condon point  $R_C = 2931$  bohrs when the detuning equals  $-5.3$  MHz. The probability for being in the excited state increases as  $R(t)$  approaches  $R_C$  from  $R > R_C$ . As  $R(t)$  decreases significantly below the crossing radius, the population begins to decrease drastically. Below  $R = 2000$  bohrs, oscillations in excited-state population are superimposed on the generally decreasing excited-state population. Figure 2 actually plots the results of two different calculations using different trajec-

TABLE I. Kinetic energies for the three choices of excited-state trajectories.

	Asymptotic	Energy conserving	Switched
$R = R_C$	$T_g(\infty) - V_a(R)$	$T_g(\infty) - \hbar\Delta - V_a(R)$	$T_g(\infty) - \hbar\Delta - V_a(R)$
$R = \infty$	$T_g(\infty)$	$T_g(\infty) - \hbar\Delta$	$T_g(\infty)$

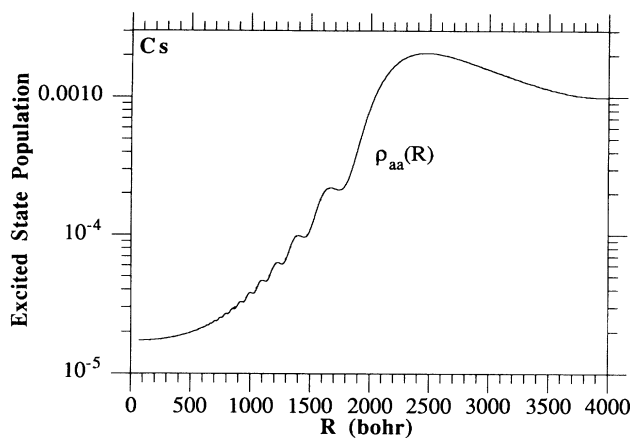


FIG. 2. Excited-state population  $\rho_{aa}(R)$  vs internuclear distance  $R$ . The calculation is for  $l=0$ ,  $\Delta=-5.3$  MHz, and  $T=9.5 \times 10^{-10}$  Ry (0.3 mK),  $I=1.4 \times 10^{-5}$  W/cm<sup>2</sup>. Two different calculations using different trajectories are shown, as described in the text. The results are practically indistinguishable.

jectories. The first calculation solves Eqs. (2.11) and (2.13) for the trajectory on the ground-state potential, using the corresponding correction factor for the excited state, and the second calculation solves for the trajectory on the excited-state potential with the corresponding correction factor for the ground-state trajectory. The differences in the results are negligible and can hardly be seen in the figure, despite the fact that the actual trajectories are radically different, as evident in Fig. 3 which plots  $R(t)$  versus time for the two different potentials. It is for this reason that we plot our results for the excited-state population  $\rho_{aa}$  and the coherence  $\rho_{ag}$  versus  $R$ , and not time. Figure 4 compares the excited-state populations obtained using the correction factors which are trajectory independent (solid curve) with the results using no correction factor and propagating on the ground- and on the excited-state trajectories. The excited-state population obtained without correction factors and using the ground-state tra-

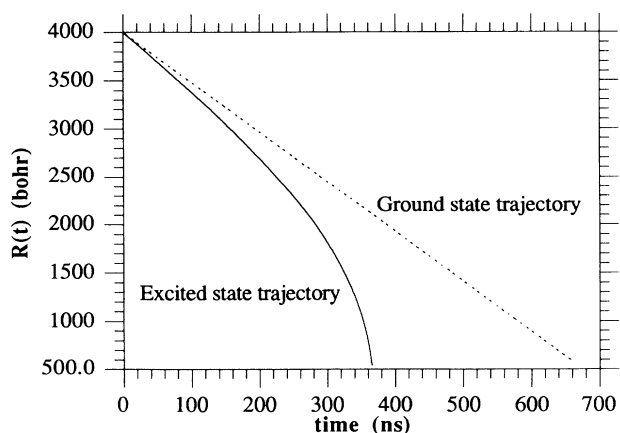


FIG. 3.  $R(t)$  vs time for the ground- and excited-state potentials for the parameters of Fig. 2.

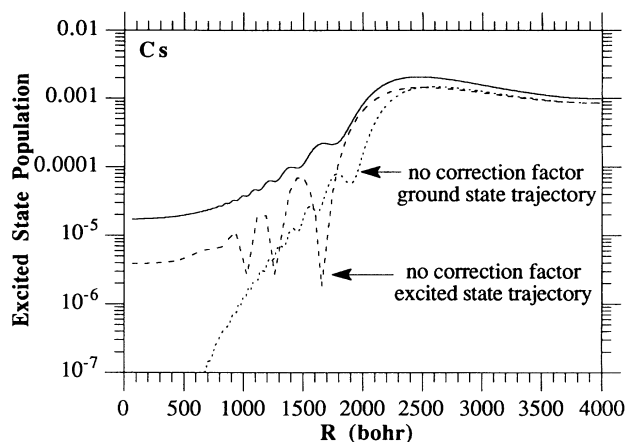


FIG. 4. Comparison of excited-state population vs internuclear distance for  $l=0$ ,  $\Delta=-5.3$  MHz, and  $T=9.5 \times 10^{-10}$  Ry (0.3 mK),  $I=1.4 \times 10^{-5}$  W/cm<sup>2</sup> computed with correction factors and without correction factors using ground- and excited-state trajectories.

jectory decays more rapidly than it should because the ground-state velocity is slower than the actual velocity on the excited state. The excited-state population obtained without correction factors and using the excited-state trajectory decays as it should but is reduced because less time is spent being excited from the ground state. (The slight discrepancy between the results at  $R=4000$  arises because the correction factors are not quite unity at  $R=4000$  due to small nonvanishing excited-state potential, and the “asymptotic” values of  $\rho_{ij}$  were computed at  $R=4000$  with these nonunity correction factors. We could have started the calculation at larger  $R$  thereby reducing this discrepancy.)

Figure 5 shows the coherence,  $\text{Im}[\rho_{ag}(R)]$ , which drives the difference in population,  $\rho_{gg} - \rho_{aa}$ ; this quantity is proportional to the rate of excitation of population [see Eq. (2.25)].  $\text{Im}[\rho_{ag}(R)]$  peaks at about  $R=2600$  bohrs (as opposed to the steady-state coherence which peaks at

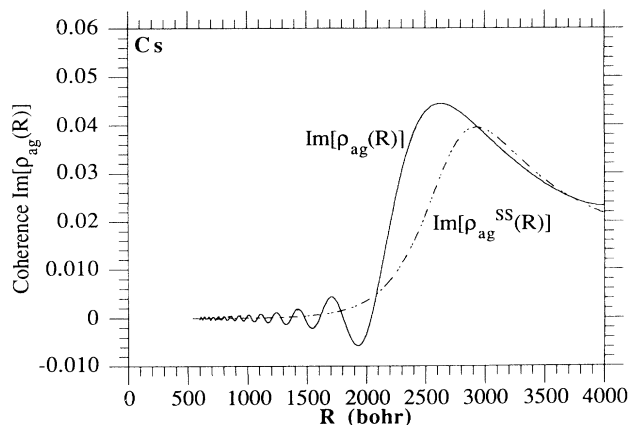


FIG. 5  $\text{Im}[\rho_{ag}(R)]$  vs internuclear distance  $R$ . Also shown is the steady-state value of this coherence,  $\text{Im}[\rho_{ag}^{\text{SS}}]$ . The calculation is for  $l=0$ ,  $\Delta=-5.3$  MHz, and  $T=9.5 \times 10^{-10}$  hartree (0.3 mK),  $I=1.4 \times 10^{-5}$  W/cm<sup>2</sup>.

$R_C$  for weak laser fields) and then rapidly decreases before beginning to oscillate rapidly around a value of zero for  $R$  less than about 2000 bohrs. Also shown in the figure is the steady-state value of this coherence,  $\text{Im}[\rho_{ag}^{SS}]$ , versus internuclear distance.  $\text{Im}[\rho_{ag}^{SS}]$  and the calculated value  $\text{Im}[\rho_{ag}]$  have much in common.  $\text{Im}[\rho_{ag}^{SS}]$  passes through the oscillations in  $\text{Im}[\rho_{ag}]$  at small  $R$ , and the quantities are very similar at large  $R$ . However, the temporal variation of the coherence as a function of  $R$  is too rapid for good agreement with the steady-state values of  $\text{Im}[\rho_{ag}^{SS}]$  in the region  $2000 < R < 3000$  bohrs. The oscillations in  $\text{Im}[\rho_{ag}]$  about zero and its zero average value are due to the large detuning  $\delta(R) = \omega_{21}(R) - \omega_0$ . (The slight discrepancy between  $\rho_{ij}^{SS}$  and  $\rho_{ij}$  at  $R = 4000$  arises for the same reasons stated in the preceding paragraph.)

Figure 6 compares the calculated excited-state population  $\rho_{aa}(R, l, \Delta, \phi)$  versus  $R$  with the steady-state excited-state population  $\rho_{aa}^{SS}(R, l, \Delta, \phi)$ , the population  $P_{ga}^{JV}(R, l, \Delta, \phi)$ , and the population  $P_{ga}^{OBE}(R, l, \Delta, \phi)$  determined using the numerically calculated  $\rho_{ag}(R, l, \Delta, \phi)$  as described in Eq. (2.28). The steady-state population and the calculated population are similar at large  $R$ , but at smaller  $R$ ,  $\rho_{aa}^{SS}$  decrease with decreasing  $R$  much faster than  $\rho_{aa}$ . The excited-state population is not in steady state and the decay of the population is considerably slower than the steady-state approximation yields. The population  $P_{ga}^{JV}$  behaves much more similarly to the population  $\rho_{aa}$  than the steady-state approximation. The decay of the excited state as calculated by the semiclassical excited-state survival factor (2.20) contains the right physics to describe the decay. Nevertheless, there are significant differences between the  $P_{ga}^{JV}$  and  $\rho_{aa}$ . At small  $R$  and near the peak of the excited-state population at  $R \approx 2600$  bohrs the differences are quite apparent. Upon using Eq. (2.26) for  $G_{ga}^{OBE}(R)$  in Eq. (2.22) to obtain  $P_{ga}^{OBE}$ , improved agreement with  $\rho_{aa}$  is obtained.

We now consider higher relative angular momentum channels. When  $l > 0$ , propagation of the OBE's is stopped for  $R < R_g(l)$ , the turning point on the ground-

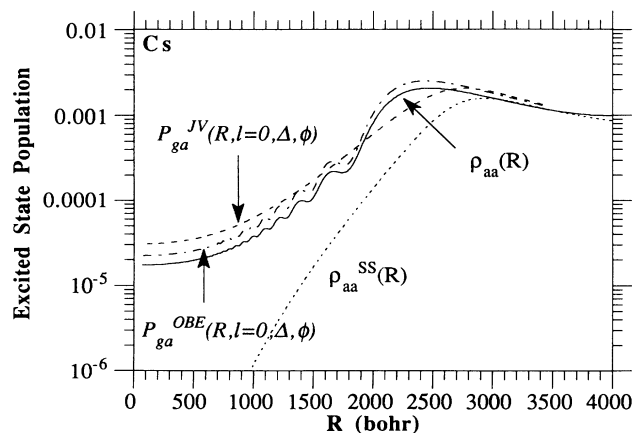


FIG. 6. Excited-state population  $\rho_{aa}(R)$ , steady-state excited-state population  $\rho_{aa}^{SS}(R)$ , population  $P_{ga}^{JV}(R, l, \Delta, \phi)$ , and population  $P_{ga}^{OBE}(R, l, \Delta, \phi)$  vs  $R$ . The calculation is for  $l=0$ ,  $\Delta = -5.3$  MHz, and  $T = 9.5 \times 10^{-10}$  hartree (0.3 mK),  $I = 1.4 \times 10^{-5}$  W/cm<sup>2</sup>.

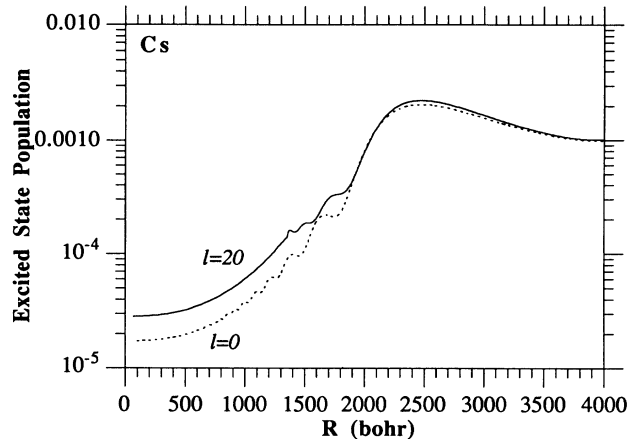


FIG. 7. Excited-state population  $\rho_{aa}(R)$  vs internuclear distance for  $l=20$ ,  $\Delta = -5.3$  MHz, and  $T = 9.5 \times 10^{-10}$  hartree (0.3 mK),  $I = 1.4 \times 10^{-5}$  W/cm<sup>2</sup>.

state potential. No excitation is allowed for  $R < R_g(l)$  and the dynamics only involves decay. Figure 7 shows the excited-state population versus internuclear distance for  $l=20$ , and the  $l=0$  excited state is also shown for comparison. The small peak in  $\rho_{aa}$  at  $R \approx 1400$  bohrs arises due to the classical turning point on the ground-state potential for collisions with relative angular momentum  $l$  at this  $R$ . The velocity near a classical turning point on the ground state for finite  $l$  becomes slow as the probability of excitation to the excited state increases near the turning point. The population at small  $R$  is enhanced for  $l > 0$  because of the longer time spent absorbing near the turning point on the ground-state trajectory. Figure 8 shows the excited-state population versus internuclear distance for  $l=40$ , the population  $P_{ga}^{JV}(R, l, \Delta, \phi)$ , and the population  $P_{ga}^{OBE}(R, l, \Delta, \phi)$  calculated using Eq. (2.26) for  $G_{ga}^{OBE}(R)$  in Eq. (2.22) to obtain  $P_{ga}^{OBE}$ . Here the peak due to the classical turning point on the ground-state potential is much more pronounced and it occurs at larger  $R$  because of the larger  $l$ . Again, the  $P_{ga}^{OBE}$  shows fairly good agreement with the calculated

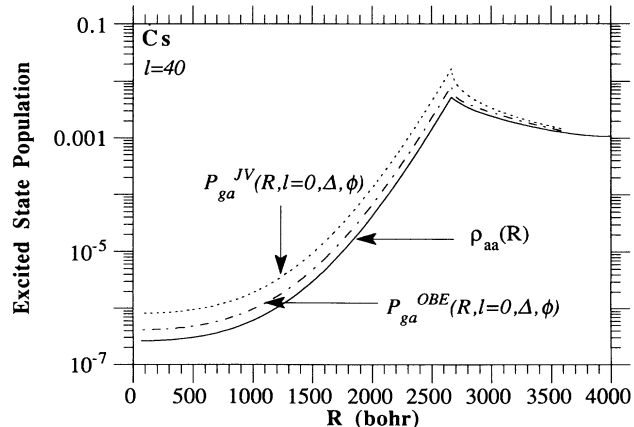


FIG. 8. Excited-state population  $\rho_{aa}(R)$  vs internuclear distance for  $l=40$ ,  $\Delta = -5.3$  MHz, and  $T = 9.5 \times 10^{-10}$  hartree (0.3 mK),  $I = 1.4 \times 10^{-5}$  W/cm<sup>2</sup>.

$\rho_{aa}$ . For  $l=40$ , the probability  $\rho_{aa}(R_X, l, \Delta, \phi)$  is already very small and it continues to decrease with increasing  $l$ . The cutoff in  $l$  is numerically performed in analogy with the discussion in JV and is determined by either ground- or excited-state trajectory considerations, depending upon detuning [10].

We now change the laser intensity to the regime where saturation becomes significant. The laser intensity is taken to be 0.07 and 35 mW/cm<sup>2</sup>. The laser detuning is not changed, and we initially consider  $l=0$ . Figure 9 shows the OBE excited-state population versus internuclear distance for these intensities. The 0.07 mW/cm<sup>2</sup> result looks like the low intensity result shown in Fig. 2, but the population is higher, whereas at 35 mW/cm<sup>2</sup> the populations are highly saturated asymptotically, and the behavior of the populations as a function of internuclear coordinate is significantly different, e.g., the oscillations of population with internuclear distance does not occur. Also shown as dashed curves are the OBE results using the excited-state reference trajectory with the appropriate correction factor, and as is evident, the results are almost indistinguishable (except inside 1250 bohrs for 35 mW/cm<sup>2</sup> where there is a small discrepancy that is due to integration inaccuracies). Figure 9 also compares  $\rho_{aa}(R)$  with  $P_{ga}^{JV}(R, l, \Delta, \phi)$  for the high intensity case. At high intensities, the population  $P_{ga}^{JV}(R, l, \Delta, \phi)$  does not follow  $\rho_{aa}(R)$  at large  $R$ , since the JV model is a weak-field model which does not take into account the finite asymptotic value of the excited-state population or the strong-field coupling occurring during the collision. The expression for  $P_{ga}^{JV}(R, l, \Delta, \phi)$  overestimate the excited-state population at large  $R$  because the excitation rate is calculated assuming all the population is in the ground state.

If the asymptotic choice in Table I is made, the formulation for the correction factors in Eq. (2.2'') insures that the  $\{C_k(R)\}$  are asymptotically equal to unity. In other words, the asymptotic kinetic energy on the excited-state surface is taken equal to the kinetic energy on the

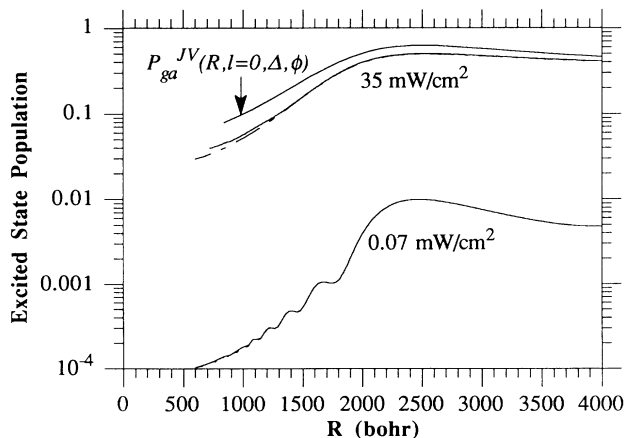


FIG. 9. Excited-state population  $\rho_{aa}(R)$  vs internuclear distance,  $R$  for two different intensities,  $I=0.07$  and 35 mW/cm<sup>2</sup>, and  $l=0$ ,  $\Delta=-5.3$  MHz  $T=9.5 \times 10^{-10}$  hartree (0.3 mK). Two different calculations using different trajectories are shown, as described in the text. The results are practically indistinguishable.

ground-state surface. The rationale for this is that upon asymptotic absorption of a photon and excitation of the ground state to the excited state the kinetic energy does not change, even if the detuning of the laser frequency from resonance is large. However, what happens to the kinetic energy if a photon is absorbed at finite  $R$ ? In particular, what happens to the kinetic energy if the photon is absorbed at the Condon point  $R_C(\Delta)$ ? The local velocity on the ground-state trajectory is given by  $v_g(R_C)=[2\mu\{T-[\epsilon_g(R_C)-\epsilon_g(\infty)]\}]^{1/2}$ , whereas the local velocity on the excited state is given by  $v_a(R_C)=[2\mu\{T-[\epsilon_g(R_C)-\epsilon_g(\infty)]\}]^{1/2}$ . Thus the local kinetic energies on the two channels are not equal at the Condon point. This does not correspond to the usual assumption that the local velocity does not change if the optical transition occurs at the Condon point. The switched correction factor choice described in Sec. II F and Table I takes the velocity on the excited-state trajectory equal to

$$v_a(R) = \begin{cases} v_g(R) & \text{for } R > R_C \\ [2\mu\{T-[\epsilon_a(R)-\epsilon_a(\infty)-\hbar\Delta]\}]^{1/2} & \text{for } R \leq R_C \end{cases} \quad (3.1)$$

and thus, the correction factors depend on the detuning for  $R \leq R_C$ , and the CFCP is satisfied at  $R_C$ . We have numerically computed the dynamics using such switched correction factors. Figure 10 shows for the weak-field case and small detuning,  $\Delta=\gamma_{ga}$ , the results of the three different trajectory choices indicated in Table I. These choices affect the way the correction factors are calculated, and lead to different results, even though, for a given choice, running ground- or excited-state trajectories give the same results. The curve labeled ‘‘asymptotic’’ corresponds to the choice used in Figs. 2–9. For this choice the excited-state kinetic energy is the highest throughout the trajectory, so survival tends to be better. The curve labeled ‘‘switched’’ is smaller in magnitude, since survival is less because of the slower motion on the excited-state potential. The curve labeled ‘‘energy conserving’’ has a choice equivalent to the ‘‘switched’’ choice for  $R < R_C$ , but is unphysical in that the ground and excited states

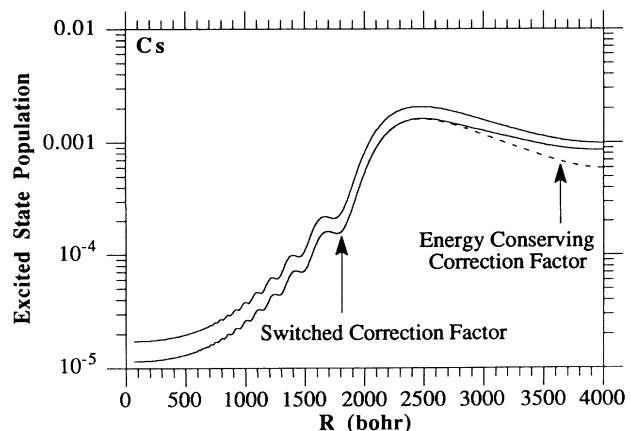


FIG. 10. Switched, energy conserving, and asymptotic correction factor results for  $\rho_{aa}(R)$ , for  $l=0$ ,  $\Delta=-5.3$  MHz,  $T=9.5 \times 10^{-10}$  hartree (0.3 mK), and  $I=1.4 \times 10^{-5}$  W/cm<sup>2</sup>.

evolve with different velocities as  $R \rightarrow \infty$ . Because the velocity in the excited state is too low at large  $R$ , it has poorer survival from large  $R$ . However, since most of the excitation for the Cs case comes with  $R < R_C$ , where the “switched” and “energy conserving” trajectories are equivalent, both give essentially the same results for the probability  $\rho_{aa}(R)$  at small  $R$ .

### B. Fine-structure rates versus detuning and intensity

Figure 11 shows the calculated FS contribution to the trap loss rate coefficient, as a function of red detuning for a total laser intensity of  $10 \text{ mW/cm}^2$ . The rate coefficient is  $2K_g$ , where  $K_g$  is calculated from Eq. (2.16), since two atoms are lost from the trap for each FS transition. Results are shown for the “asymptotic” and “switched” trajectory choices discussed in relation to Table I. For small detunings,  $\Delta = \gamma_{ga}$ , the two methods give similar results. However, the rate for the former rises faster than the rate for the latter as detuning increases. The “asymptotic” choice violates the CFCP at  $R_C$ , brings the atoms together too fast, and causes the survival factor to be too large. Although the “switched” and “energy conserving” trajectories in Table I are equivalent for  $R < R_C$ , the “switched” trajectory is to be preferred to the “energy conserving” one, since when  $\hbar\Delta \gg kT$ , the excited-state kinetic energy for the latter is negative or nonclassical over much of the long-range part of the trajectory where  $R > R_C$ . Figure 11 also shows the result of the JV formula, calculated with the “L” approximation of JV, for which the excited-state survival factor, Eq. (2.20), was found by assuming the CFCP is satisfied at each  $R$  at which excitation occurs.

Figure 12 compares the calculated rate coefficients versus laser intensity with the data points reported by

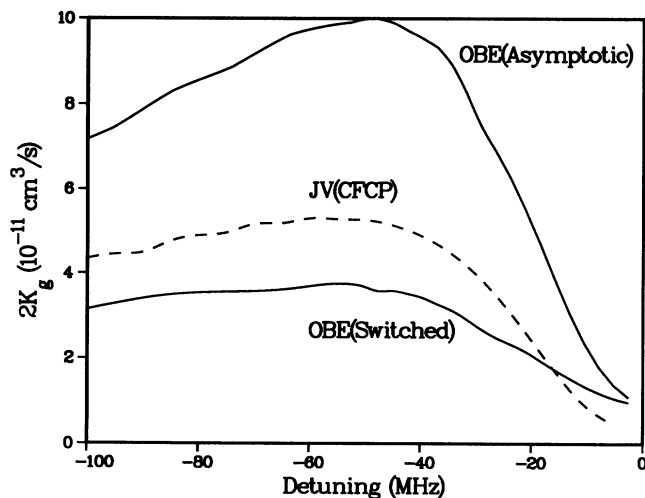


FIG. 11. Trap loss rate vs detuning calculated using asymptotic and switched correction factors for laser intensity  $I = 10 \text{ mW/cm}^2$ . Also shown is the JV result assuming the CFCP is satisfied at each  $R$  at which excitation occurs.

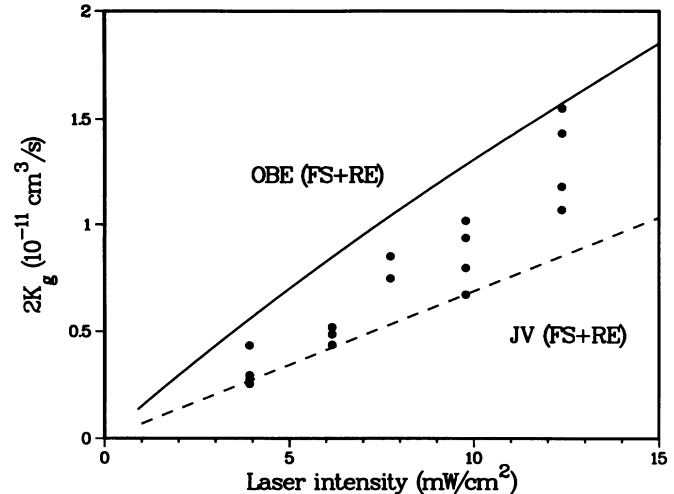


FIG. 12. Trap loss rate vs laser intensity for  $\Delta = -5.3 \text{ MHz}$ . The points show the data of Sesko *et al.* [9].

Sesko *et al.* [9] due to ground- plus excited-state collisions in a magneto-optical Cs trap at about  $300 \mu\text{K}$ . The FS contribution was calculated using the OBE theory with the “switched” trajectory correction factors. We added to this the smaller RE contribution calculated by the JV theory [10]. The results of the JV calculation is also shown in the figure, where the JV survival factors were calculated as for Fig. 11, that is, the CFCP is satisfied at each  $R$  at which excitation occurs. Since most of the excitation in the JV theory comes from the region with  $R < R_C$ , the survival factors tend to be smaller in the JV theory than in our OBE calculation, and the JV rate coefficient lies below our OBE result. The data are bracketed by the two results.

The near-linear intensity dependence indicated by the data in Fig. 12 is also reproduced by the OBE calculation (the JV theory is a weak-field theory inherently linear in intensity). The Rabi frequency  $\Omega$ , defined by Eqs. (2.7) and (2.27), equals one molecular linewidth,  $\gamma_{ga}$ , at an intensity of  $36 \text{ mW/cm}^2$ . The atomic on-resonance saturation intensity is about an order of magnitude less. Although the experimental power is above the atomic saturation intensity, our calculations show the molecular transition is not yet saturated. Careful examination of Fig. 12 shows that the OBE curve does show some curvature, implying the beginning of saturation. Moreover, the slope of the OBE curve at very low intensities is larger than the apparent linear slope seen in Fig. 12. At an intensity of  $40 \text{ mW/cm}^2$  the calculated rate is only about half of that found by assuming the linear intensity dependence extrapolated from the slope of the calculations with power  $\leq 2 \text{ mW/cm}^2$ . Since the FS mechanisms are very different in the various alkali-metal species, we might expect the saturation properties of trap loss might also vary among alkali-metal species, a conclusion indicated by preliminary calculations on trapped Na.

Sesko *et al.* [9] also reported the result of a “catalysis” laser experiment, in which the loss rate was enhanced by the addition of a second “catalysis” laser in addition to the trapping lasers. Figure 13 shows our calculated loss rate versus catalyst laser detuning for the parameters of the experiment, namely, a total trap laser power of 13 mW/cm<sup>2</sup> and detuning of  $\Delta = \gamma_{ga}$  and a catalysis laser power of 24 mW/cm<sup>2</sup>. The RE contribution of the JV theory was added to the FS contribution from the OBE calculations for the detuning-independent background due to presence of the trapping lasers, and the FS loss rate due to the catalysis laser was added to that. Switched trajectories were used to calculate the correction factors in the OBE calculation. The figure also shows the calculated catalysis laser contributions of the JV and GP theories. The GP results were calculated from Eqs. (36) and (37) of the JV paper [10], that is, the same molecular potentials and parameters were used as for the JV theory. Both JV and GP results are calculated assuming the local CFCP is satisfied at the point of excitation.

Figure 13 shows basically good agreement between the theory and experiment. Sesko *et al.* [9] had also reached this conclusion on the basis of their application of the GP theory. We also see that the OBE, JV, and GP theories approach one another in the limit of large detuning, although there are appreciable differences in the detuning range  $-300$ – $0$  MHz. The agreement at large detuning is expected as a consequence of Eq. (2.31), from which the GP expressions can be derived as a limiting case at large detuning for weak fields. At large red detuning, but not so large that discrete bound-state structure becomes significant, the excitation is localized in a small region near the Condon point and all three theories give equivalent results.

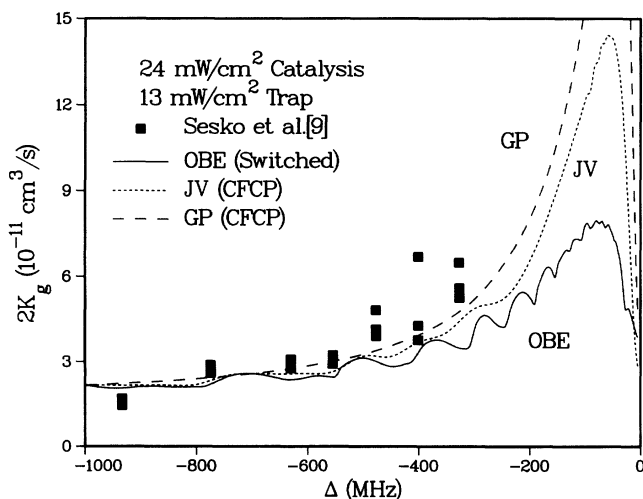


FIG. 13. Trap loss rate vs “catalysis” laser detuning for the conditions of the experiment in Sesko *et al.* [9]. Total trap laser power of 13 mW/cm<sup>2</sup> and detuning of  $\Delta = \gamma_{ga}$  and a catalysis laser power of 24 mW/cm<sup>2</sup>. The points show the experimental data.

#### IV. SUMMARY AND CONCLUSION

The optical-Bloch-equation approach developed here incorporates a molecular picture of the atomic collision, laser-field dressing of the molecular states participating in the dynamics, and decay of the population and polarization due to spontaneous emission. The relative motion degree of freedom is treated semiclassically in the sense that an appropriate trajectory is used for each channel. This leads to a trajectory-independent method. The present approach incorporates the correct molecular aspects of the collision, the dissipation which causes decay of the population and the coherence as the dynamics of the system evolves, the saturation of the optical transition when the laser field is not weak, the multichannel aspects of the trap loss process, and the non-steady-state character of the optical excitation as the internuclear coordinate changes. It reduces to the JV theory when the steady-state approximation is made and the weak-field limit is taken. An application of the method to Cs trap loss due to fine-structure-changing collisions is presented. Good agreement with experiment is obtained. The method can be adapted to also calculate radiative escape trap loss, autoionization trap loss, and redistribution of radiation. However, there are aspects of cold-atom collision in optical traps that are not properly treated in the present formulation. Cold-atom collisions in optical traps can produce ground-state atoms having different asymptotic kinetic energy than they had before the collision, i.e., the energy of the matter and laser field is not conserved because of the interaction with the spontaneous emission degrees of freedom that are so important in such collisions. Similarly, excited-state atoms with different asymptotic kinetic energy can be produced. Any approach (e.g., close coupling of optically dressed states) which conserves energy in the matter–laser-field subsystem cannot properly account for the spread of asymptotic kinetic energies which occurs because of the interaction with the spontaneous emission degrees of freedom. Although the GP, JV, and OBE models can incorporate aspects of this spread within their semiclassical framework, it seems that to correctly model this aspect of the collision dynamics, a time-dependent density-matrix wavepacket approach is needed with the kinetic energy treated as an operator [32], i.e.,

$$\frac{d}{dt}\rho(R, R'; t) = -\frac{i}{\hbar}[H(R)\rho(R, R'; t) - \rho(R, R'; t)H(R')] - \Gamma\rho,$$

where  $\mathbf{H}(R) = T(R)1 + V(R)$ , is a differential operator because of the nuclear kinetic-energy term. It is clear that a wealth of new physics is present in the study of cold-atom collisions occurring in optical traps, and much new physics remains to be uncovered.

#### ACKNOWLEDGMENTS

We thank Dr. R. J. Bieniek for useful and stimulating discussions and suggestions. P.S.J. wishes to thank the Institute for Theoretical Atomic and Molecular Physics

for support through a grant from the National Science Foundation while visiting the Harvard-Smithsonian Center for Astrophysics; he also wishes to thank the Office of Naval Research for partial support. This work

was partially supported by the National Science Foundation through a grant for the Institute for Theoretical Atomic and Molecular Physics at Harvard University and Smithsonian Astrophysical Observatory.

- 
- [1] J. Vigué, *Phys. Rev. A* **34**, 4476 (1986).
- [2] H. R. Thorsheim, J. Weiner, and P. S. Julienne, *Phys. Rev. Lett.* **58**, 2820 (1987).
- [3] P. S. Julienne, *Phys. Rev. Lett.* **61**, 698 (1988).
- [4] P. S. Julienne, S. H. Pan, H. R. Thorsheim, and J. Weiner, in *Advances in Laser Science, Vol. 3*, Proceedings of the Third International Laser Science Conference, Atlantic City, NJ, 1987, AIP Conf. Proc. No. 172, edited by A. C. Tam, J. L. Gole, and W. C. Stwalley (AIP, New York, 1988), p. 308.
- [5] P. L. Gould, P. D. Lett, P. S. Julienne, W. D. Phillips, H. R. Thorsheim, and J. Weiner, *Phys. Rev. Lett.* **60**, 788 (1988).
- [6] M. Prentiss, A. Cable, J. E. Bjorkholm, S. Chu, E. L. Raab, and D. E. Pritchard, *Opt. Lett.* **13**, 452 (1988).
- [7] P. S. Julienne and F. H. Mies, *J. Opt. Soc. Am. B* **6**, 2257 (1989).
- [8] A. Gallagher and D. E. Pritchard, *Phys. Rev. Lett.* **63**, 957 (1989).
- [9] D. Sesko, T. Walker, C. Monroe, A. Gallagher, and C. Wieman, *Phys. Rev. Lett.* **63**, 961 (1989).
- [10] P. S. Julienne and J. Vigué, *Phys. Rev. A* **44**, 4464 (1991).
- [11] P. D. Lett, P. S. Jessen, W. D. Phillips, S. L. Rolston, C. I. Westbrook, and P. L. Gould, *Phys. Rev. Lett.* **66**, 2139 (1991).
- [12] P. S. Julienne and R. Heather, *Phys. Rev. Lett.* **67**, 2135 (1991).
- [13] A. Gallagher, *Phys. Rev. A* **44**, 4249 (1991).
- [14] A. M. Smith and K. Burnett, *J. Opt. Soc. Am. B* **8**, 1592 (1991).
- [15] R. A. Broglia, S. Landowne, R. A. Malfiet, V. Rostokin, and Aa. Winther, *Phys. Rep.* **11**, 1 (1974).
- [16] G. Gabrielse and Y. B. Band, *Phys. Rev. Lett.* **39**, 697 (1977); Y. B. Band, *Phys. Rev. A* **19**, 1906 (1979); *J. Phys. B* **12**, 2359 (1979); *Phys. Rev. A* **21**, 1152 (1980); *J. Chem. Phys.* **72**, 2881 (1980); *J. Phys. B* **13**, 3215 (1980). See also M. S. Child, *Molecular Collision Theory* (Academic, London, 1976).
- [17] Y. B. Band and P. S. Julienne (unpublished).
- [18] J. Dalibard and C. Cohen-Tannoudji, *J. Opt. Soc. Am. B* **2**, 1707 (1985).
- [19] A. Aspect, E. Armondo, R. Kaiser, N. Vansteenkiste, and C. Cohen-Tannoudji, *J. Opt. Soc. Am. B* **6**, 2112 (1989).
- [20] P. J. Ungar, D. S. Weiss, E. Riis, and S. Chu, *J. Opt. Soc. Am. B* **6**, 2058 (1989); E. Riis, D. S. Lewis, K. A. Moler, and S. Chu, *Phys. Rev. Lett.* **64**, 1658 (1990).
- [21] J. von Neumann, *Mathematical Foundations of Quantum Mechanics* (Princeton University Press, Princeton, NJ, 1955).
- [22] L. Allen and J. H. Eberly, *Optical Resonance and Two Level Atoms* (Dover, New York, 1987), Chap. 7.
- [23] V. Weisskopf and E. Wigner, *Z. Phys.* **63**, 54 (1930); J. R. Ackerhalt, P. L. Knight, and J. H. Eberly, *Phys. Rev. Lett.* **30**, 456 (1973); J. R. Ackerhalt and J. H. Eberly, *Phys. Rev. D* **10**, 3350 (1974).
- [24] J. J. Sakurai, *Advanced Quantum Mechanics* (Addison-Wesley, Reading, MA, 1967), Chap. 2.
- [25] R. Bavli, D. F. Heller, and Y. B. Band, *J. Chem. Phys.* **91**, 6714 (1989).
- [26] Y. B. Band and P. S. Julienne, *J. Chem. Phys.* **94**, 5291 (1991).
- [27] R. J. Bieniek, *J. Chem. Phys.* **72**, 1225 (1980).
- [28] W. J. Meath, *J. Chem. Phys.* **48**, 227 (1968).
- [29] The detuning cannot be too large, or excited-bound-state structure becomes important, as discussed in Refs. [10] and [12].
- [30] P. S. Julienne and F. H. Mies, *Phys. Rev. A* **34**, 3792 (1986).
- [31] W. J. Alford, K. Burnett, and J. Cooper, *Phys. Rev. A* **27**, 1310 (1983).
- [32] M. Berman, R. Kosloff, and H. Tal-Ezer (unpublished).
- [33] P. S. Julienne, A. M. Smith, and K. Burnett, in *Advances in Atomic, Molecular and Optical Physics*, edited by D. R. Bates and B. Bederson (Academic, San Diego, 1992).